JOURNAL OF GEOPHYSICAL RESEARCH, VOL. 113, A05213, doi:10.1029/2007JA012856, 2008

Analysis of plasma waves observed within local plasma injections seen in Saturn's magnetosphere

J. D. Menietti,[1] O. Santolik,[2] A. M. Rymer,[3] G. B. Hospodarsky,[1] A. M. Persoon,[1] D. A. Gurnett,[1] A. J. Coates,[4] and D. T. Young[5]

Received 4 October 2007; revised 29 November 2007; accepted 4 February 2008; published 17 May 2008.

[1] Plasma injections or density depletion regions have been reported to be a prolific feature of Saturn's inner magnetosphere. They are characterized by flux tubes of warm, tenuous plasma in a cooler, locally produced plasma background. The injected plasma undergoes dispersion in energy due to gradient and curvature drifts as the flux tube transports. The plasma waves within these injections are of at least two types. Above the electron cyclotron frequency, f_{ce}, very intense and narrow-banded emissions resembling electrostatic cyclotron harmonics (ECH) are often observed. Below f_{ce}, whistler mode chorus is sometimes observed. Inside the plasma injections there exists a low-energy (<100 eV) electron component which tends to have a field-aligned pitch angle distribution, and a warmer (E > 1000 eV) component with "pancake" pitch angle distributions (peaked at 90°). We model the electron plasma distributions observed inside one injection to conduct a linear dispersion analysis of the wave modes. The results suggest that the ECH emissions can be generated by phase space density gradients associated with a narrow loss cone that is likely to be present but not observed because the electron detectors field of view did not include the magnetic field line at the time of the observations. The whistler mode chorus emission can be generated by the pancake-like distribution and temperature anisotropy ($T_\perp/T_\parallel > 1$) of the warmest plasma population. Some interesting anomalies between the results and the observations may be resolved by analyses of additional injection events.

Citation: Menietti, J. D., O. Santolik, A. M. Rymer, G. B. Hospodarsky, A. M. Persoon, D. A. Gurnett, A. J Coates, and D. T. Young (2008), Analysis of plasma waves observed within local plasma injections seen in Saturn's magnetosphere, *J. Geophys. Res.*, *113*, A05213, doi:10.1029/2007JA012856.

1. Introduction

[2] *Hill et al.* [1981] and *Pontius et al.* [1986] have discussed radial transport of plasma in a rotation-dominated magnetosphere as exists at Jupiter and at Saturn. A consequence of this model is the interchange instability by which distant magnetic flux tubes containing low-density, warm plasma transport inward to interchange with cooler, more dense, outward convecting magnetic flux tubes. *Burch et al.* [2005] and *Hill et al.* [2005] presented evidence of this phenomena for the specific case of Saturn's magnetosphere using Cassini Plasma Spectrometer (CAPS) observations of injected plasma events with significant plasma energy dispersion due to $\mathbf{E} \times \mathbf{B}$ longitudinal drift.

[3] These plasma injections consist of a cool, low-energy component (E < 100 eV) with a tendency to have a field-aligned pitch angle distribution (PAD) (peaked at 0 and 180°), and a warmer, higher-energy component (E > 1000 eV) with a "pancake" PAD (peaked at 90°). The warm pancake component is consistent with a scenario wherein outer magnetospheric plasma is adiabatically transported inward. Given its field-aligned character the origin of the contained cold component could be linked to the planetary ionosphere, whereas the cold electrons outside the plasma injection are produced locally from Saturn's icy satellites and rings [*Rymer et al.*, 2007, 2008]. Intense plasma waves are observed that can provide insight not only to the observed plasma populations but also "hidden" plasma at pitch angles and/or energies beyond the limits of the electron low-energy spectrometer (ELS).

[4] Plasma injection events are frequently observed by the Cassini spacecraft in the range 6 to ~12 R_S (R_S = Saturn radius) and similar hot plasma injection phenomena have been observed near the Io torus at Jupiter [e.g., *Frank and Paterson*, 2000; *Thorne et al.*, 1997; *Mauk et al.*, 1997, 1999, 2002]. *André et al.* [2007] describe how the events described in this paper are manifest in several of the in situ Cassini instruments. Within the plasma injections the Radio

[1]Department of Physics and Astronomy, University of Iowa, Iowa City, Iowa, USA.
[2]Institute of Atmospheric Physics, ASCR, and Charles University, Prague, Czech Republic.
[3]Johns Hopkins University, Applied Physics Laboratory, Laurel, Maryland, USA.
[4]University College London, Mullard Space Science Laboratory, Dorking, UK.
[5]Southwest Research Institute, San Antonio, Texas, USA.

Copyright 2008 by the American Geophysical Union.
0148-0227/08/2007JA012856$09.00

and Plasma Wave Science instrument (RPWS) typically observes intense electrostatic cyclotron harmonics (ECH) and often whistler mode emissions. ECH emissions at frequencies between the harmonics of f_{ce}, $f \sim (n + 1/2)f_{ce}$ are typically observed in the terrestrial magnetosphere near the magnetic equator and interact strongly with keV electrons [*Kurth et al.*, 1979; *Horne and Thorne*, 2000]. In a seminal work, *Ashour-Abdalla and Kennel* [1978] thoroughly discuss the role of loss cones in the generation of ECH emissions for a full range of plasma parameters, loss cone widths and depths. *Horne and Thorne* [2000] and *Horne et al.* [2003] have shown the effectiveness of "pancake" electron PADS and temperature anisotropies ($T_\perp/T_{||} > 1$) in exciting whistler mode and chorus emission at Earth; and of narrow (a few degrees) loss cones in generating ECH emissions. These latter authors show that, for the terrestrial case, ECH waves effectively scatter electrons into the loss cone.

[5] At Earth, intense, diffuse whistler mode hiss at frequencies typically less than a few kHz is observed within the plasmasphere and is generally believed to be generated by a temperature anisotropy in the electron phase space distribution. Natural emissions of discrete, whistler mode chorus at Earth consist of electromagnetic waves in the frequency range from a few hundreds of hertz to several kHz observed in the lower-density plasmapause region. These emissions are most often characterized as narrow-banded at $f < f_{ce}/2$ and/or $f > f_{ce}/2$ with an emission gap near $f_{ce}/2$. It is generally believed that chorus is generated by a nonlinear process based on the electron cyclotron resonance of whistler mode waves with energetic electrons, taking place close to the geomagnetic equatorial plane [*Omura et al.*, 1991; *Nunn et al.*, 1997; *LeDocq et al.*, 1998; *Santolik et al.*, 2004a; *Trakhtengerts et al.*, 2004]. Storm-time chorus is especially important for the physics of the Earth's magnetosphere since it can significantly influence the distribution functions of the energetic electrons in the outer radiation belt [e.g., *Meredith et al.*, 2003; *Horne and Thorne*, 2003]. Observations of chorus emission at Saturn have recently been reported by *Hospodarsky et al.* [2007].

[6] In this paper we report on the plasma and wave observations within one plasma injection event with particular interest in explaining the free energy sources of the observed plasma waves. We model the electron distribution function to show that ECH emissions similar to those observed can be generated by assuming a narrow loss cone. Whistler mode emissions at frequencies somewhat lower than the observed chorus emissions can be excited by the observed pancake distribution with a temperature anisotropy. The results suggest a direction for future work to resolve some of the discrepancies between the observations and the model calculations.

2. Instrumentation

2.1. RPWS

[7] The Cassini Radio and Plasma Wave Science (RPWS) instrument measures oscillating electric fields over the frequency range 1 Hz to 16 MHz and magnetic fields in the range 1 Hz to 12 kHz [*Gurnett et al.*, 2004]. The instrument uses three nearly orthogonal electric field antennas (the E_u and E_v antennas have an opening angle of about 130°) and three orthogonal magnetic search coil antennas, providing a direction-finding capability. There are five receiver systems: the high frequency receiver (HFR) covering 3.5 kHz to 16 MHz; the medium frequency receiver (MFR) covering 24 Hz to 12 kHz; a low frequency receiver (LFR) covering 1 Hz to 26 Hz; a 5-channel waveform receiver which operates in either a 1–26 Hz or 3 Hz to 2.5 kHz mode; and a high resolution wideband receiver that covers two frequency bands, 60 Hz to 10.5 kHz and 800 Hz to 74 kHz. The data presented in this study utilize all of the receivers.

2.2. ELS

[8] The Cassini Plasma Spectrometer (CAPS) is composed of three sensors: the electron spectrometer (ELS), the ion beam spectrometer (IBS), and the ion mass spectrometer (IMS). Of importance in this study is the ELS which consists of an eight-detector fan array in a single plane. Each detector has a 5.2° × 20° field of view for a total in-plane field of view of 160°. The instrument measures electron energy from 0.6 eV to 28,250 eV over a period of 2 s with a resolution of $\Delta E/E = 0.17$ [*Young et al.*, 2004].

3. Observations

[9] We present electron spectrometer data depicting the electron population of an injection region. In Figure 1 we show an energy-versus-time spectrogram of differential energy flux obtained by ELS. The data were obtained on 30 October 2005, from 0730 to 0750 UT, and clearly show the signature of a plasma injection within the approximate time range of 0735:20 to 0740:20 UT. During this time period the satellite is at a latitude of 0.39°, and the local time (*LT*) and radius (*r*) are in the approximate range 23.20 h < *LT* < 23.22 h and 7.00 $R_S < r <$ 7.04 R_S. Within the injection, the low-energy flux is greatly reduced while flux for electrons with $E > 1$ keV is enhanced. At lower energies the distribution is more field-aligned, while at higher energies there is a distinct pancake-like population. In Figure 2 we plot contours of the electron phase space distribution in velocity space. Figure 2a displays the more pancake-like distribution at higher energies ($E < 26$ keV), while Figure 2b shows the more field-aligned (cigar-shaped) distribution at lower energies ($E < 285$ eV). During this time period there were no observations along the magnetic field line. The smallest observed pitch angles were greater than about 15 degrees. In Figure 3 we have plotted the plasma density as determined from the moments of the ELS phase space distribution. The density of the lower-energy population ($E < 100$ eV) is always greater, but the higher-energy electrons are generally within a factor of two. These values of density are also consistent with observations of the upper hybrid frequency shown below.

[10] In Figure 4 we present the low-rate electric field intensity in a frequency versus time spectrogram. The data extend from 0720 to 0800 UT over the frequency range 0 to 60 kHz. The white line indicates the upper hybrid frequency, f_{uH}, and thus can be used to obtain the electron density. Within the plasma injection region the upper hybrid frequency is much lower (the arrow indicates what is

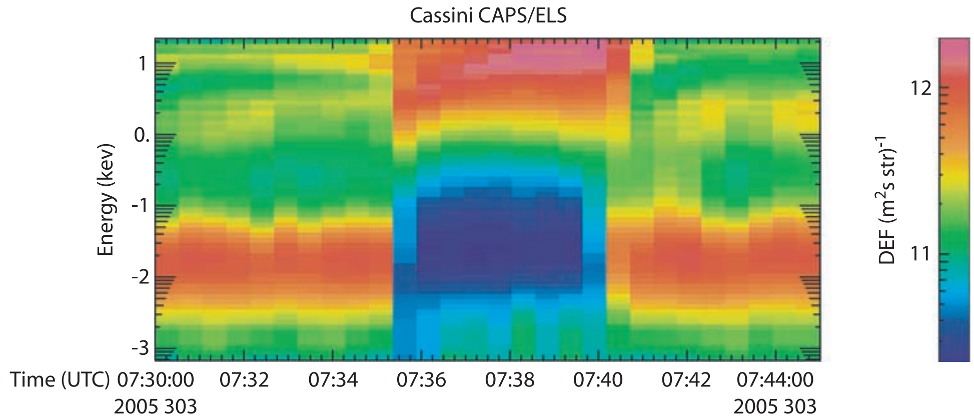

Figure 1. An energy-versus-time spectrogram of differential energy flux obtained by ELS. The data were obtained on 30 October 2005 from 0730 to 0750 UT and show the signature of a plasma injection in the approximate time range of 0735:20 to 0740:20 UT. Within this time range, the low-energy flux is greatly reduced while flux for electron flux for $E > 1$ keV is enhanced.

interpreted as f_{uH} within the injection at a frequency of about 20 kHz), and there are a number of banded ECH emissions at $f < 15$ kHz. The RPWS also obtained high-resolution wideband data in the 10 kHz bandwith mode for this time period. In Figure 5 we display this data obtained during the injection region. Now the white line indicates the electron cyclotron frequency, f_{ce}. The banded emission is more clearly resolved as a series of emissions separated by approximately f_{ce} ($\sim$1300 Hz determined from the magnetometer data), which we identify as electrostatic cyclotron harmonic (ECH) emission. Indicated by the arrows are two bands of emission that appear to be independent from the other ECH bands. These two emission bands appear to have a different source from the other ECH bands, and this emission extends beyond the injection region shown in Figure 5. This emission is also seen throughout Figure 4 just above f_{ce}. Since this emission is not unique to the injection region and is probably independent of it, it will be the subject of another study.

[11] Whistler mode emission is observed below f_{ce}, which includes intense, narrowband emissions which are indicative of chorus as reported by *Hospodarsky et al.* [2007]. This can be verified by the waveform receiver data also obtained at this time. We used the Means method [cf. *Means*, 1972; *LeDocq et al.*, 1998] to analyze the spectral waveforms for $f < 1$ kHz. In Figure 6 we display an analysis spectrogram of the 5-channel waveform receiver data showing the electric and magnetic fields as well as the wave normal directions for the emission observed within the plasma injection region. The panels contain (top to bottom) electric field; magnetic field; wave normal angle (θ) relative to the magnetic field; and the wave direction (red is toward the magnetic equator, indicating a source at higher latitude). The intense chorus emission propagates in at least two bands, the lower band ranges from about 450 Hz to about 600 Hz. A higher-frequency band during the second half of the injection period exists in the range from about 670 Hz to about 740 Hz. The calculated wave normal angle displayed in the third panel indicates values ranging from 0 to near 90 degrees. The wave polarization (not shown) is calculated to be right-hand circular. These two bands of right-handed polarized emission with a narrow gap near $f_{ce}/2$ strongly support the identification of whistler mode chorus.

4. Wave Growth Rate Analysis

[12] We have fitted the observed ELS electron distribution function contours using a sum of bi-Maxwellians as follows:

$$f_s(v_\perp, v_\parallel) = \sum_S \left(\frac{n_S}{\pi^{\frac{3}{2}} w_{\perp S}^2 w_{\parallel S}} \right) \left[(1-\Delta_S) e^{-\frac{v_\perp^2}{w_{\perp S}^2}} + \frac{\Delta_S}{1-\beta_S} \left(e^{-\frac{v_\perp^2}{w_{\perp S}^2}} - e^{-\frac{v_\perp^2}{\beta_S w_{\perp S}^2}} \right) \right] e^{-\left(\frac{(v_\parallel - v_{ds})^2}{w_{\parallel S}^2} \right)}, \quad (1)$$

where n_s is the density, $v_\parallel$ and $v_\perp$ are the particle velocities parallel and perpendicular to the magnetic field, respectively; $w_\parallel$ and $w_\perp$ are the parallel and perpendicular thermal velocities, respectively; v_d is the parallel drift velocity. The parameters Δ and β describe the depth and width of the model loss cone, respectively. Other choices of a fitting function, such as a power law kappa distribution perhaps could have been chosen, however, the sum of Maxwellians, with large number of fitting parameters, provides a good fit to the data as will be shown. We use a nonlinear least squares fitting routine to fit the model to the data. We have assumed five populations of plasma, four electron distributions, and a cold plasma ion distribution. The electron populations include a cool core plasma, a midenergy plasma, a higher-energy warm plasma, and a very cold background plasma. The ions are assumed to be a cold background. In Table 1 we present the fitting parameters determined near the center of the plasma injection region. We initially adjusted and fixed the thermal velocity of the cold background plasma (which has an energy less than the lowest energy of the ELS) to a value which allowed the bandwidth of the fundamental ECH band to be close to that observed.

[13] The PADs were sampled at various points throughout the plasma injection and a time near the center of the region

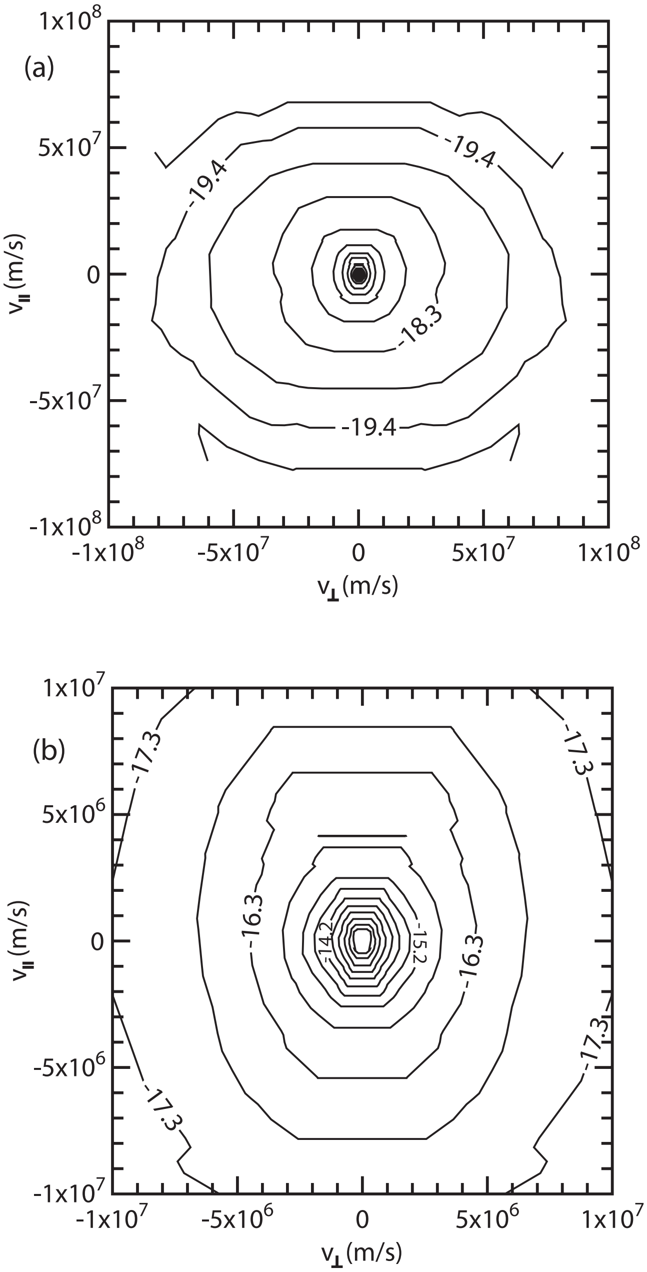

Figure 2. Contours of the logarithm of electron phase space distribution in velocity space (s^3/m^6). Figure 2a displays the more pancake-like distribution at higher energies (up to 26 keV), while Figure 2b (at higher resolution and E < 285 eV) shows the more field-aligned (cigar-shaped) distribution at lower energies.

was selected as being characteristic of the event with modest changes of the temperature aniostropy in the high energy distribution being the most notable difference. In Figure 7 we overplot contours of the model electron distribution function and the actual data. The loss cone of the cool core distribution is critical for the generation of the ECH emissions. The higher-energy pancake-like distribution and the temperature anisotropy are responsible for the growth of the whistler mode chorus emissions at low frequency. To estimate the size of the loss cone near the magnetic equator we note that Saturn kilometric radio emissions are observed up to ~1 MHz. This emission is believed to due to the cyclotron maser instability and requires a source of electrons. Assuming a magnetic field as given by *Connerney et al.* [1983], and a mirror point near an altitude in the polar region where $f_{ce} \sim 1$ MHz we estimate a loss cone of less than 3 degrees for $L \sim 7$, near the position of the observed plasma injection close to the magnetic equator. Such a loss cone would not be visible to the ELS instrument during the time of the observations. In Figure 8, at higher resolution, we plot contours of the model distribution including a narrow loss cone of approximately 3 degrees or less which lies too close to the magnetic field line to be observed by the ELS instrument.

4.1. ECH Emissions

[14] We have used a modification of a warm plasma dispersion solver [cf. *Santolik and Parrot*, 1996], based on the susceptibility tensor calculated by the program, waves in homogeneous, anisotropic multicomponent plasmas (WHAMP) [cf. *Ronnmark*, 1982; 1983] to determine roots of the dispersion equation and calculate the growth rate of the plasma waves resulting from the model distribution function. The solver also includes a cold plasma susceptibility tensor, which we used for the background ion component. In Figure 9 we display the results for the ECH emissions at the fundamental, first and second harmonic frequencies. This plot shows the real part of the frequency versus wave number in the lower panel and the imaginary part of the frequency relative to f_{ce} in the upper panel. The wave normal angle that produced the largest growth rate for the fundamental, first, and second harmonic emission was 89.3°, 89.6°, and 89.7°, respectively. The maximum growth is ~0.031 f_{ce} for f_{real} = 1473 Hz at the fundamental with a bandwidth extending from ~1400 Hz to ~1620 Hz. The observed emission near the fundamental appears to extend from about f_{ce} (1300 Hz) to about 1640 Hz, which is close to the modeled bandwidth. For the first harmonic emission the maximum growth is 0.025 f_{ce} for f_{real} = 2755 Hz with a

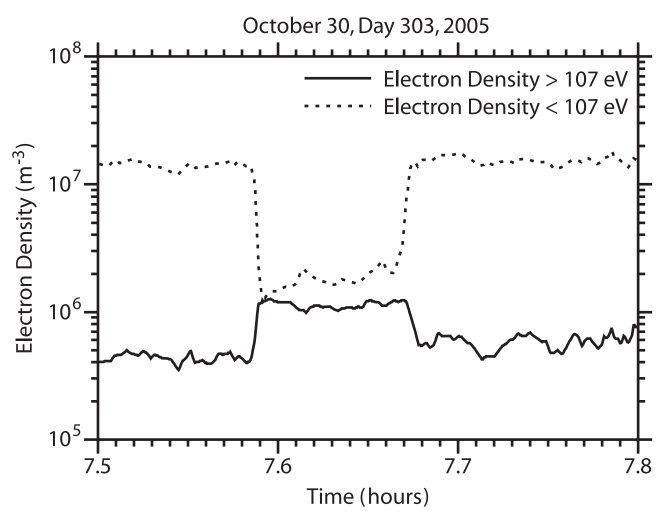

Figure 3. The plasma density as determined from the moments of the ELS phase space distribution is plotted. The lower-energy population (E < 100 eV) is always greater in density, but the density of the higher-energy electrons is generally within a factor of two.

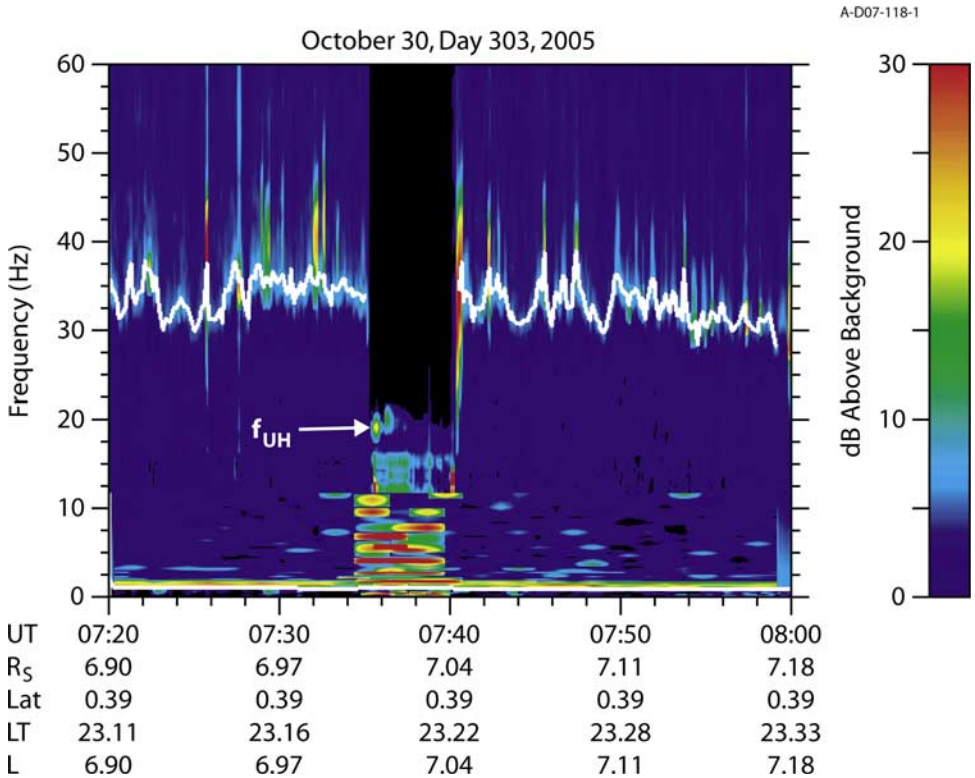

Figure 4. A frequency versus time spectrogram of the low-rate electric field intensity is presented. The data extend from 0720 to 0800 UT over the frequency range 0 to 60 kHz. The white line indicates the upper hybrid frequency, f_{uH}, and thus can be used to obtain the electron density. Within the plasma injection region the upper hybrid frequency is much lower (arrow), and there are a number of banded ECH emissions at $f < 15$ kHz.

bandwidth extending from ~2690 Hz to ~2915 Hz. The observed bandwidth appears to extend from about 2700 Hz to about 3100 Hz, a larger bandwidth than modeled. For the second harmonic emission the maximum growth is 0.019 f_{ce} for f_{real} = 4041 Hz with a bandwidth extending from ~3985 Hz to ~4150 Hz. The observed bandwidth extends from ~4000 Hz to ~4450 Hz, also larger than that modeled.

[15] Growth of the ECH emission is dependent on the phase space density gradient provided by the loss cone. The pancake-like distribution at higher energies without the loss cone is insufficient to drive the ECH emission. Increasing the width of the loss cone in the cool core distribution only, by adjusting β in equation (1) upward to 0.05 (Δ = 1.0, θ = 89.3°) initially increases then decreases the growth rate of the fundamental and harmonic emission but also slightly decreases the bandwidth. For β = 0.01 in the cool core and cold electron populations, the loss cone angle is less than 3° for all energies. When β is increased to 0.05, the loss cone width approaches 3° degrees for $E > 15$ eV and increases to ~5° at $E \sim 10$ eV and ~10° for $E < 2$ eV. Decreasing the depth of the loss cone for the cool core distribution by adjusting Δ downward to 0.5 (β = 0.01, θ = 89.3°) decreases the growth rate and also decreases the bandwith. For Δ = 1.0 the loss cone extends to the lowest energies, but as Δ decreases, the loss cone is "filled" to higher and higher energies while the width remains constant. We display these effects in Figures 10 and 11. Independently adjusting these same parameters by similar amounts in the other distribution populations had almost no affect on the growth rates.

[16] We can estimate the signal gain produced by these growth rates. From the calibrated observations we estimate the maximum signal strength of the ECH emission to be about 30 dB above background. For the growth rate calculations of the fundamental emission shown in Figure 9 the group velocity of the wave is about 5×10^{-4} c almost along the magnetic field and $\omega_i \sim 0.02\ f_{ce}$ so the path length required to produce 30 dB of gain is about 7 km. This is quite short and easily obtained within the injection region, which has a dimension perpendicular to the magnetic field line of about 3000 km. Saturation of this emission could be accomplished by pitch angle scattering and filling of the loss cone as discussed by *Horne et al.* [2003]. The latter authors have modeled pitch angle scattering due to ECH waves for a terrestrial substorm. They find that these waves are very effective at scattering electrons into the loss cone, and provide the major contribution to diffuse auroral precipitation for a substorm event observed near the magnetic equator. The diffusion time was found to be comparable to the duration of the event, consistent with the theory that filling of the loss cone by pitch angle scattering can saturate the wave growth.

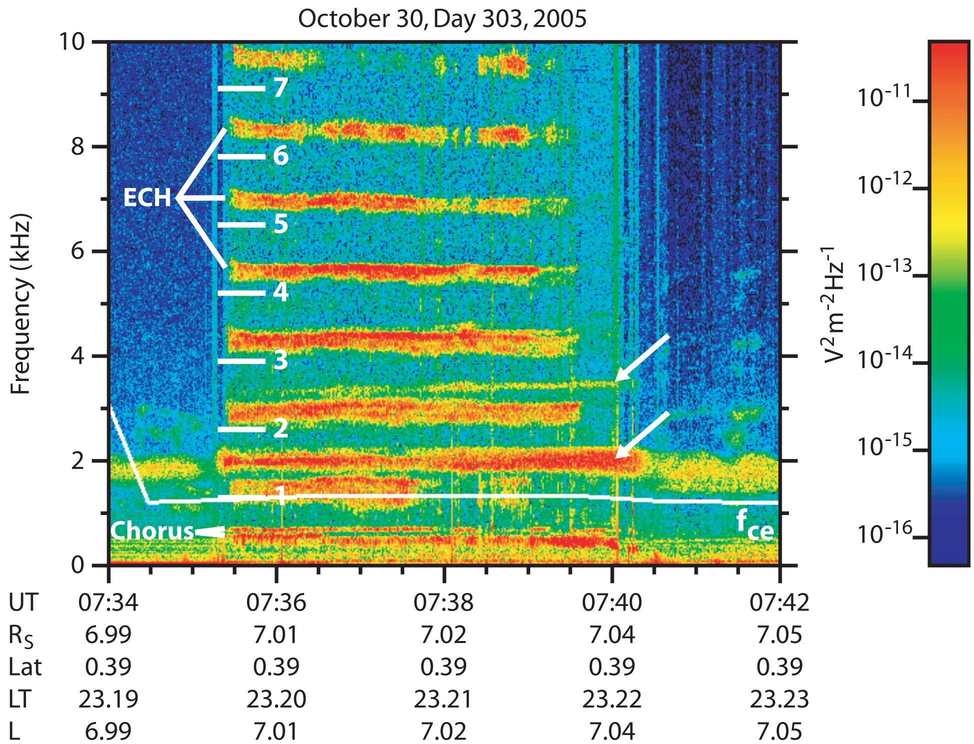

Figure 5. Electric field intensity of the ECH emission measured by the high-resolution wideband receiver for f < 10 kHz obtained during the injection region. The white line indicates the electron cyclotron frequency, f_{ce}. Indicated by the arrows are two bands of emission that appear to be independent from the other ECH bands. These two emission bands appear to have a different source from the other ECH bands, and this emission extends beyond the injection region shown in the figure.

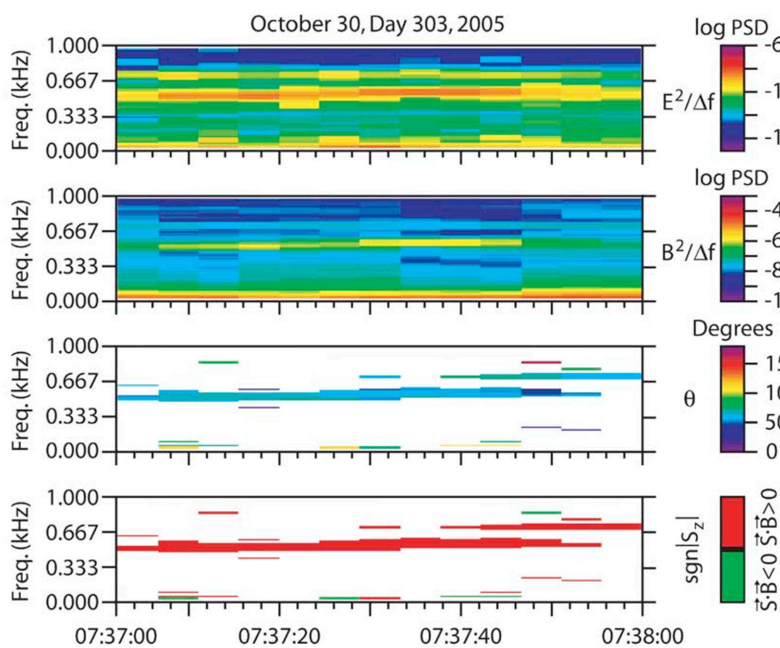

Figure 6. A spectrogram of the waveform receiver data showing the electric and magnetic field intensities and wave normal directions for the emission observed within the plasma injection region. The panels contain (top to bottom) electric field; magnetic field; wave normal angle (θ) and the wave direction (red is toward the magnetic equator).

Table 1. Plasma Fitting Parameters

	Density[a] (%)	$w_{\parallel}$ (eV)	$T_{\perp}/T_{\parallel}$	V_d (eV)	Δ	β
Cold background	5.0	0.178	1.0	0	1.0	0.01
Cool core	72.0	5.93	0.46	0	1.0	0.01
Mid-E	5.5	543	0.59	0	1.0	0.001
Hi-E	17.5	1.83×10^4	1.53	0	1.0	0.001
Cold ions	100	cold				

[a]Total density is 4.69 cm^{-3}.

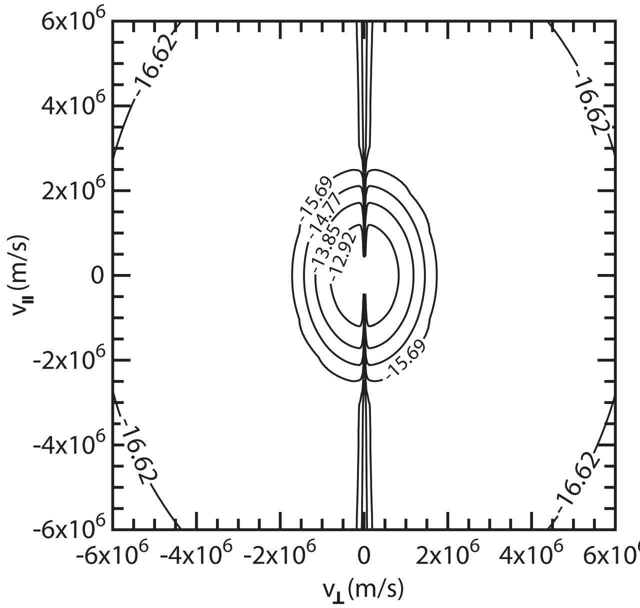

Figure 8. At higher resolution (E < 100 eV), we plot contours of the model distribution including a narrow loss cone of approximately 3 degrees.

4.2. Whistler Mode Emissions

[17] The same electron distribution function shown in Figures 7 and 8 is also unstable to the growth of whistler mode emission at small wave normal angles. The critical parameters include the wave normal angle, θ, and the magnitude of the temperature isotropy. The free energy source is the higher-energy, pancake-like distribution. We have calculated the growth rates for chorus emission again using the distribution function fitting parameters of Table 1. In Figure 12 we plot the real (imaginary) part of the frequencies as before in the bottom (upper) panels. The middle panel displays the index of refraction as cB/E. The whistler mode emission is seen to grow for frequencies in the approximate range 40 Hz < f < 130 Hz, with higher growth rates for wave normal angles less than about 10 degrees. The peak growth rate is about 0.3% $f_{\rm real}$ for $f_{\rm real}$ = 105 Hz and $\theta = 1°$. For $\theta = 10°$, the peak growth rate decreases to 0.13% $f_{\rm real}$ for $f_{\rm real}$ = 104 Hz. Note the growth rates are shown relative to the real frequency rather than f_{ce} as for the ECH emissions. In Figure 13 we show the effect of changing the value of the temperature anisotropy, $T_{\perp}/T_{\parallel}$, for the high-energy pancake-like distribution only. In this plot the upper panel shows the growth rate increases as $T_{\perp}/T_{\parallel}$ varies from the fitted value of 1.5 (used also in Figure 12) to 1.7, 2.0, and 2.25. These values may represent reasonable variations of $T_{\perp}/T_{\parallel}$ associated with temporal changes during the plasma injection event. The wave normal angle was held constant at 1° for each curve shown in Figure 13. The growth is seen to increase substantially with increasing values of $T_{\perp}/T_{\parallel}$, with a peak at $\sim$1.5% $f_{\rm real}$ for $f_{\rm real}$ = 150 Hz. The maximum frequency of the whistler mode growth also increases to over 200 Hz and the allowed wave normal angles increase to over 15 degrees. Increasing $T_{\perp}/T_{\parallel}$ to 3.0 increases the maximum frequency of emission to about 250 Hz and allowable wave normal angles increase to over 20 degrees.

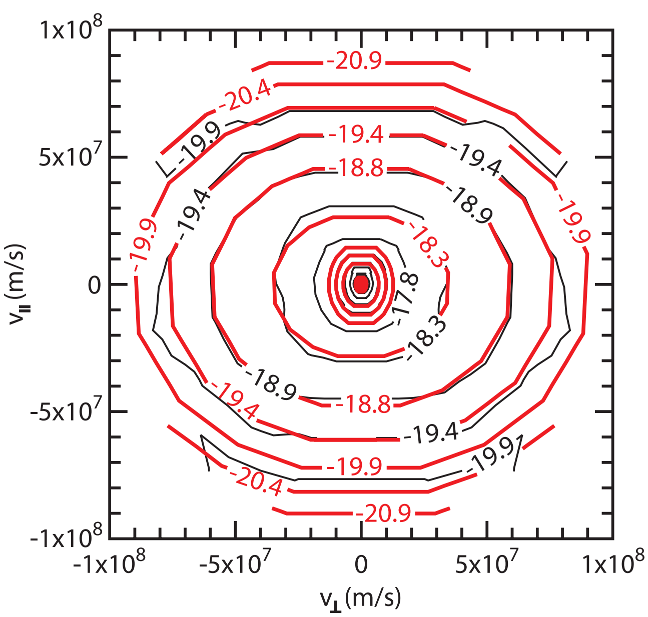

Figure 7. Contours of the model electron distribution function are overplotted (red) with contours of the observed phase space distribution. The plot is for all energies (E < 27 keV) and the units of the contours are s^3/m^6.

[18] We estimate the signal gain produced by these whistler mode growth rates. The maximum signal strength for the chorus observations is also about 30 dB above background as determined from the calibrated measurements. The growth rates of the whistler mode vary from about ω_i = 1.3 rad/s for the case of $T_{\perp}/T_{\parallel}$ = 1.5 to ω_i = 14 rad/s for $T_{\perp}/T_{\parallel}$ = 2.25, with $v_g \approx 3 \times 10^{-2}$ c along the magnetic field, so the required path length to obtain 30 dB of growth would range from about 5000 km to 49,000 km. This length is much larger than for the ECH emissions and larger than the approximate dimension of the injection region perpendicular to the magnetic field line which we estimate to be about 3000 km. However, the chorus emissions, which are whistler mode, travel almost along the magnetic field line. Thus, there could be a problem attaining gains of 30 dB for the whistler mode if the spacecraft is less than 5000 km from the source region.

[19] The calculated frequency range of the whistler mode emission lies below the most intense bands of observed whistler mode emission displayed in Figure 6 and identified as chorus emissions. For the whistler mode emission the parallel resonant energy of the electrons varies inversely

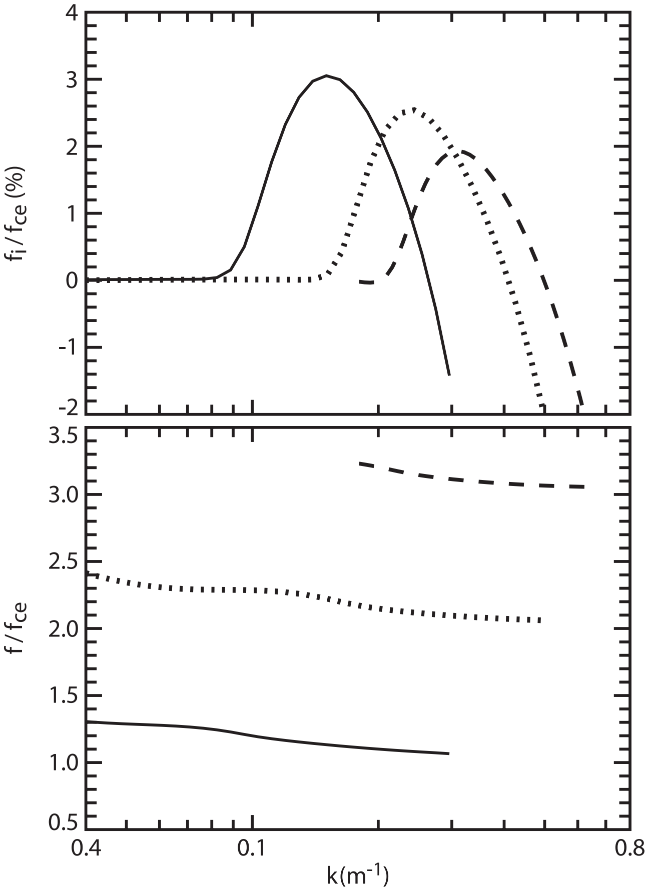

Figure 9. Results of the dispersion analysis are displayed for the ECH emissions at the fundamental, first and second harmonic frequencies. Shown are the real part of the frequency versus wave number in the lower panel and the imaginary part of the frequency relative to f_{ce} in the upper panel. The wave normal angle for the fundamental, first and second harmonic emission was 89.3°, 89.6°, and 89.7°, respectively.

with frequency [cf. *Gurnett and Bhattacharjee*, 2005, equation (9.3.52)]:

$$W_{\parallel \mathrm{Re}S} = W_c(1 - f/f_{ce})^3 (f_{ce}/f),$$

where $W_c = m_e c^2 (f_{ce}/f_{pe})^2$. For lower values of f_{pe}, electrons will resonate at higher frequencies. From Figure 3 we note that variations of f_p by up to 25% are observed within the injection region. For this reason we have recalculated the growth rate of the whistler mode emission for a lower value of f_p = 14,312 Hz. For the case of $T_\perp/T_\parallel$ = 2.25, and θ = 1°, the maximum frequency extends from about 100 Hz previously to ~300 Hz. The growth rate and maximum frequency of the whistler mode increases as the ratio $T_\perp/T_\parallel$ increases. For $T_\perp/T_\parallel$ = 4.0 the maximum frequency of growth extends to over 400 Hz, and the maximum growth rate is ~3.6% f_{real}. In Figure 14 we display the growth rate calculations for three values of $T_\perp/T_\parallel$ = 2.25, 3.0, and 4.0 for a constant θ = 1°. The growth rates are larger because of the larger values of $T_\perp/T_\parallel$, and the maximum allowed wave normal angle increases to about 25°. While values of $T_\perp/T_\parallel$ up to 4.0 are larger than those obtained from fitting the data to equation (1), they may not be unreasonable if one considers temporal effects, and the possibility that those electromagnetic emissions may be propagating from a more distant source region above the satellite within the injection.

5. Summary and Conclusions

[20] The electron distributions observed by CAPS ELS on Cassini within the plasma injection have lower density than the surrounding plasma. Cooler, more field-aligned PADs exist for E < 100 eV and warmer pancake electron PADS electrons exist for E > 1000 eV. On the basis of a parametric fit to the observed phase space densities, we have modeled the observed electrons with three separate populations as well as a cold background population below the energy range of the ELS sensor, and we have assumed the existence of a narrow loss cone. Using the linear dispersion solver [*Santolik and Parrot*, 1996], based on the susceptibility tensor calculated by the code WHAMP [*Ronnmark*, 1982, 1983], we show that a narrow loss cone within the cool core distribution can drive growth of oblique

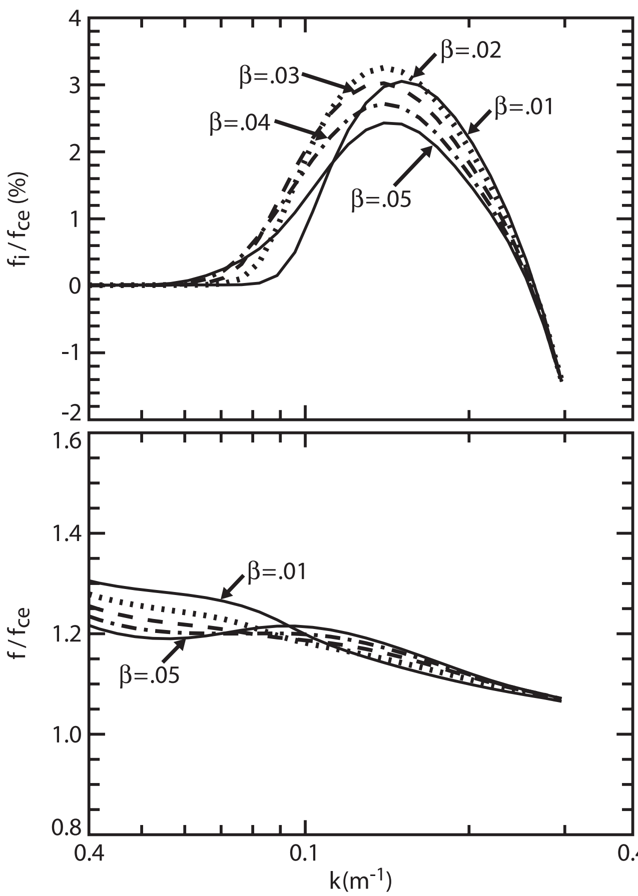

Figure 10. In the same format as Figure 9 we plot the growth rate of the fundamental emission while varying the width (β) of the loss cone for the cool core distribution and holding the depth constant (Δ = 1.0).

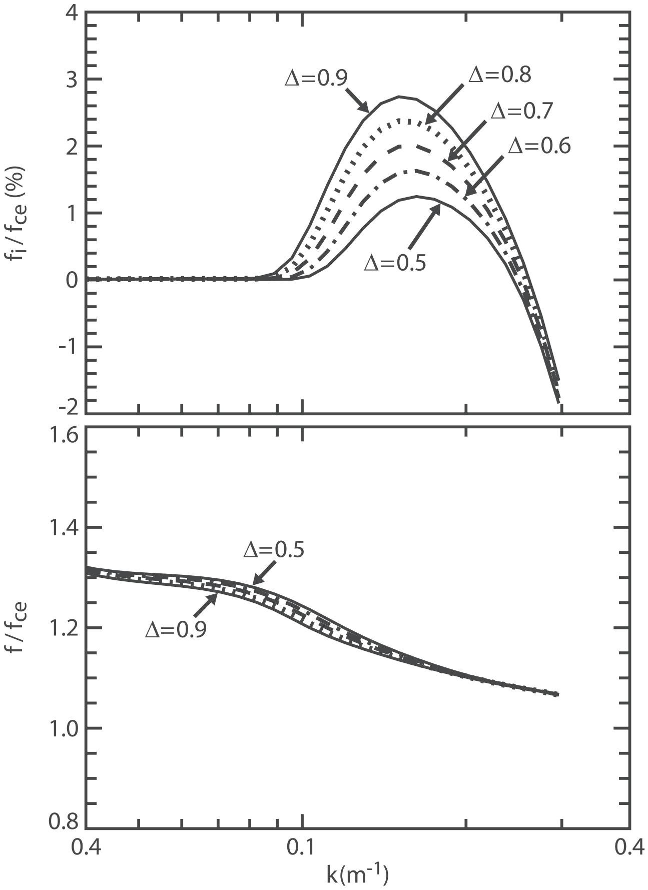

Figure 11. Same as Figure 10 but now showing the effect of decreasing the depth, Δ, of the cool core distribution loss cone, while holding the width constant (β = 0.01).

electrostatic cyclotron waves similar to those observed. That the electron loss cone is not observed is probably only because the field of view of the ELS detectors does not lie close enough to the magnetic field line direction during the event. As explained earlier, conservation of the first adiabatic invariant for mirroring electrons near the Kronian ionosphere would produce a loss cone of about 3 degrees at the magnetic equator for L = 7. The model calculations produce narrow-banded emission slightly above f_{ce} and at harmonics of f_{ce}. The bandwidths of the model harmonic ECH emissions are about 35–55% of those observed, which may be explained by temporal variations of the cyclotron frequency, thermal velocity, and density of the plasma within the injection (plasma depletion) region, as well as a range of emission wave normal angles. We also note that the modeled bandwidths were only determined at the optimum wave normal angle. A distribution of wave normal angles about the maximum will produce a larger bandwidth of ECH emission that could easily explain the small discrepancies.

[21] The higher-energy pancake-like distribution with a temperature anisotropy drives whistler mode emissions similar to those observed but at lower frequency. The intense lower band chorus emissions lie in the approximate range 450 Hz < f < 650 Hz, while the maximum frequency of whistler mode emission from the model distribution is about 215 Hz for $T_\perp/T_\parallel$ = 2.25. By assuming a lower density of the plasma within the injection region, still within the limits of the values measured (Figure 3) and allowing values of $T_\perp/T_\parallel$ up to 4.0 we can extend the maximum frequency of the whistler mode emission to over 400 Hz. The maximum observed value of $T_\perp/T_\parallel$ determined by fitting samples of the data to a Maxwellian was about 2.5. However, it may not be unreasonable to hypothesize larger values if we allow for temporal changes in the data within the injection (density depletion) region, and if we allow for the possibility that the source of the chorus emission may be located at some distance away, where the plasma distribution may be different. At Earth chorus source regions are associated with the magnetic equator, but the extent of the source region is estimated to be several thousands of kilometers [cf. *Parrot et al.*, 2003; *Santolik et al.*, 2004b], and the exact source region may be displaced from the magnetic equator. For our case at Saturn, the satellite is located near the magnetic equator. We have already seen from Figure 6 that the chorus emission is propagating from

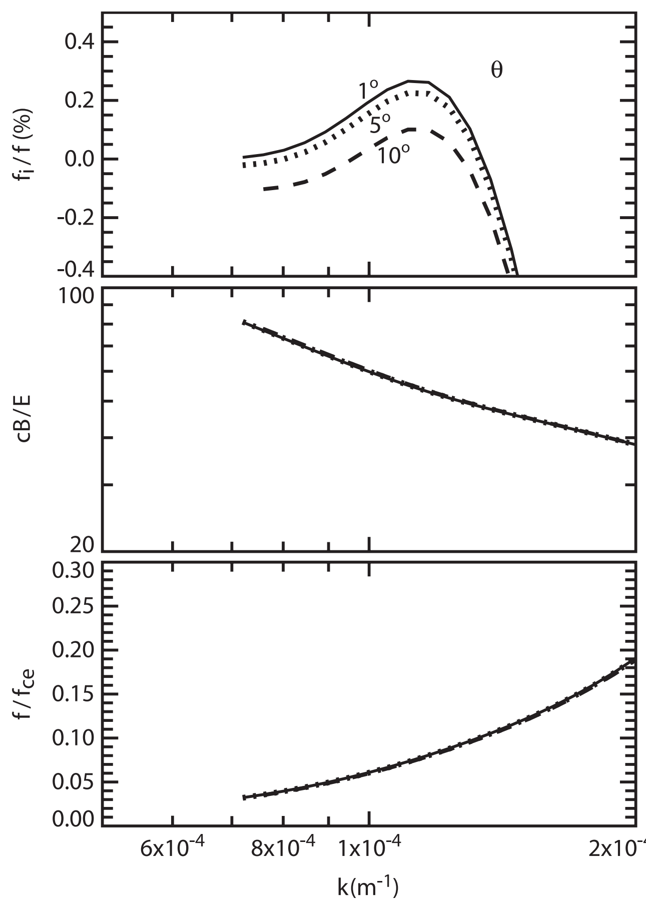

Figure 12. Results for the dispersion analysis of the whistler mode emissions are displayed for three wave normal angles. Plotted are the real (imaginary) frequencies as before in the bottom (upper) panels. The middle panel displays the index of refraction as cB/E.

a region above the satellite. As shown in terrestrial studies of chorus emission [*Parrot et al.*, 2003], satellites within a chorus source region are expected to show wave propagation from mixed directions, both toward and away from the magnetic equator. It is not inconceivable that the electron distribution observed locally within the injection region may be different from that of a chorus source location at some distance above the satellite, still within the injection region. At this location the electron distribution may be more pancake with a larger ratio of $T_\perp/T_\parallel$.

[22] As explained in section 1, the presence of the warm plasma with a pancake distribution is consistent with the interchange instability and distant, warm plasma adiabatically transported inward. The success in explaining the main features of the wave observations is encouraging and suggests a quantitative understanding of basic physical processes. The plasma waves can be fundamentally explained by a plasma distribution consistent with that hypothesized for a rotationally dominated Saturnian magnetosphere.

[23] A preliminary study of numerous other plasma injection (density depletion) events indicates that some contain ECH emissions with no chorus emissions, while others seem to contain weak or no ECH emissions. These observations along with the discrepancies found with the maximum frequency of the whistler mode growth calculations are incentives to continue further studies of additional injection events and the surrounding plasma environments. The plasma waves strongly suggest the presence of a narrow electron loss cone which was not observable by ELS due to look-direction limitations. We made note earlier of emission (shown by arrows in Figure 5) that is not unique to the injection region but extends outside this region as well. *Menietti et al.* [2002], for instance, note that electrostatic electron cyclotron emissions observed in the terrestrial polar regions can be generated by low-energy electron beams. Such beams have been observed at Jupiter and linked to auroral structure [*Mauk and Saur*, 2007], and so it is plausible that analogous processes occur at Saturn. We are particularly interested in searching for electron beams that may be responsible for some of the unexplained wave observations and may also be compatible with plasma wave injection regions that are coupled to the Kronian ionosphere.

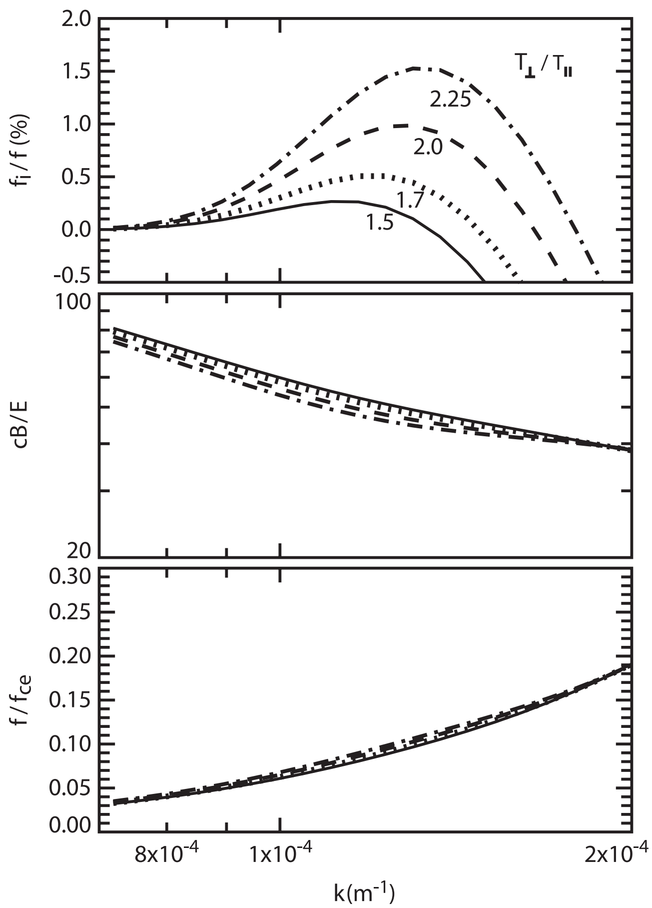

Figure 13. For the whistler mode emissions we show the effect of changing the value of the temperature anisotropy, $T_\perp/T_\parallel$, for the high-energy pancake-like distribution. The upper panel shows the growth rate increases as $T_\perp/T_\parallel$ varies from the fitted value of 1.5 (used also in Figure 12) to 1.7, 2.0, and 2.25.

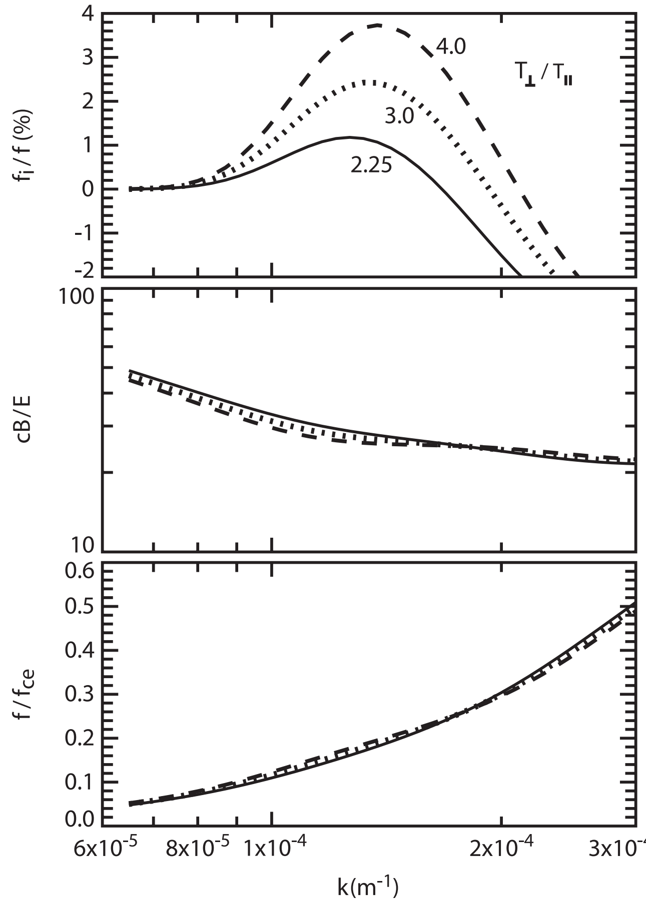

Figure 14. For a lower value of f_p = 14,312 Hz we display the growth rate calculations of the whistler mode for $T_\perp/T_\parallel$ = 2.25, 3.0, and 4.0, with $\theta = 1°$. For $T_\perp/T_\parallel$ = 4.0 the range of growth extends from about 100 Hz to over 400 Hz, and the maximum growth rate is $\sim$3.6% f_{real}.

[24] **Acknowledgments.** JDM wishes to thank Richard Horne for informative discussions of parts of this work. We thank J. Hospodarsky for clerical assistance. This work was supported by Jet Propulsion Laboratory contract 1279973 to the University of Iowa. O. S. acknowledges additional support from the ME 842 and GAAV IAA301120601 grants.

[25] Amitava Bhattacharjee thanks the reviewers for their assistance in evaluating this paper.

References

André, N., et al. (2007), Magnetic signatures of plasma-depleted flux tubes in the Saturnian inner magnetosphere, *Geophys. Res. Lett.*, *34*, L14108, doi:10.1029/2007GL030374.

Ashour-Abdalla, M., and C. F. Kennel (1978), Nonconvective and convective electron cyclotron harmonic instabilities, *J. Geophys. Res.*, *83*(A4), 1531–1543, doi:10.1029/JA083iA04p01531.

Burch, J. L., J. Goldstein, T. W. Hill, D. T. Young, F. J. Crary, A. J. Coates, N. Andre, W. S. Kurth, and E. C. Sittler Jr. (2005), Properties of local plasma injections in Saturn's magnetosphere, *Geophys. Res. Lett.*, *32*, L14S02, doi:10.1029/2005GL022611.

Connerney, J. E. P., M. H. Acuna, and N. F. Ness (1983), Currents in Saturn's magnetosphere, *J. Geophys. Res.*, *88*, 8779–8789, doi:10.1029/JA088iA11p08779.

Frank, L. A., and W. R. Paterson (2000), Observations of plasmas in the Io torus with the Galileo spacecraft, *J. Geophys. Res.*, *105*, 16,017–16,034, doi:10.1029/1999JA000250.

Gurnett, D. A., and A. Bhattacharjee (2005). *Introduction to Plasma Physics*, p. 379, Cambridge Univ. Press, Cambridge, UK.

Gurnett, D. A., et al. (2004), The Cassini radio science investigation, *Space Sci. Rev.*, *114*, 395–463, doi:10.1007/s11214-004-1434-0.

Hill, T. W., A. J. Dessler, and L. J. Maher (1981), Corotating magnetospheric convection, *J. Geophys. Res.*, *86*, 9020–9028, doi:10.1029/JA086iA11p09020.

Hill, T. W., A. M. Rymer, J. L. Burch, F. J. Crary, D. T. Young, M. F. Thomsen, D. Delapp, N. Andre, A. J. Coates, and G. R. Lewis (2005), Evidence for rotationally driven plasma transport in Saturn's magnetosphere, *Geophys. Res. Lett.*, *32*, L14S10, doi:10.1029/2005GL022620.

Horne, R. B., and R. M. Thorne (2000), Electron pitch angle diffusion by electrostatic electron cyclotron harmonic waves: The origin of pancake distributions, *J. Geophys. Res.*, *105*(A3), 5391–5402, doi:10.1029/1999JA900447.

Horne, R. B., and R. M. Thorne (2003), Relativistic electron acceleration and precipitation during resonant interactions with whistler-mode chorus, *Geophys. Res. Lett.*, *30*(10), 1527, doi:10.1029/2003GL016973.

Horne, R. B., R. M. Thorne, N. P. Meredith, and R. R. Anderson (2003), Diffuse auroral electron scattering by electron cyclotron harmonic and whistler mode waves during an isolated substorm, *J. Geophys. Res.*, *108*(A7), 1290, doi:10.1029/2002JA009736.

Hospodarsky, G. B., J. D. Menietti, T. F. Averkamp, W. S. Kurth, D. A. Gurnett, and M. K. Dougherty (2007), Whistler mode chorus observations at Saturn, poster presented at Magnetospheres of the Outer Planets 2007, Southwest Res. Inst., San Antonio, Tex.

Kurth, W. S., J. D. Craven, L. A. Frank, and D. A. Gurnett (1979), Intense electrostatic waves near the upper hybrid resonance frequency, *J. Geophys. Res.*, *84*, 4145–4164, doi:10.1029/JA084iA08p04145.

LeDocq, M. J., D. A. Gurnett, and G. B. Hospodarsky (1998), Chorus source locations from VLF Poynting flux measurements with the Polar spacecraft, *Geophys. Res. Lett.*, *25*, 4063–4066, doi:10.1029/1998GL900071.

Mauk, B. H., and J. Saur (2007), Equatorial electron beams and auroral structuring at Jupiter, *J. Geophys. Res.*, *112*, A10221, doi:10.1029/2007JA012370.

Mauk, B. H., D. J. Williams, and R. W. McEntire (1997), Energy-time dispersed signatures of dynamic injections in Jupiter's inner magnetosphere, *Geophys. Res. Lett.*, *24*, 2949–2952, doi:10.1029/97GL03026.

Mauk, B. H., D. J. Williams, R. W. McEntire, K. K. Khurana, and J. G. Roederer (1999), Storm-like dynamics of Jupiter's inner and middle magnetosphere, *J. Geophys. Res.*, *104*, 22,759–22,778, doi:10.1029/1999JA900097.

Mauk, B. H., J. T. Clarke, D. Grodent, J. H. Waite, C. Paranicas, and D. J. Williams (2002), Transient aurora on Jupiter from injections of magnetospheric electrons, *Nature*, *415*, 1003–1005, doi:10.1038/4151003a.

Means, J. D. (1972), Use of the three-dimensional covariance matrix in analyzing the polarization properties of plane waves, *J. Geophys. Res.*, *77*, 5551–5559, doi:10.1029/JA077i028p05551.

Menietti, J. D., O. Santolik, J. D. Scudder, J. S. Pickett, and D. A. Gurnett (2002), Electrostatic electron cyclotron waves generated by low-energy electron beams, *J. Geophys. Res.*, *107*(A10), 1285, doi:10.1029/2001JA009223.

Meredith, N. P., M. Cain, R. B. Horne, R. M. Thorne, D. Summers, and R. R. Anderson (2003), Evidence for chorus-driven electron acceleration to relativistic energies from a survey of geomagnetically disturbed periods, *J. Geophys. Res.*, *108*(A6), 1248, doi:10.1029/2002JA009764.

Nunn, D., Y. Omura, H. Matsumoto, I. Nagano, and S. Yagitani (1997), The numerical simulation of VLF chorus and discrete emissions observed on the Geotail satellite using a Vlasov code, *J. Geophys. Res.*, *102*(A12), 27,083–27,097, doi:10.1029/97JA02518.

Omura, Y., D. Nunn, H. Matsumoto, and M. J. Rycroft (1991), A review of observational theoretical, and numerical studies of VLF triggered emissions, *J. Atmos. Terr. Phys.*, *53*, 351–368, doi:10.1016/0021-9169(91)90031-2.

Parrot, M., O. Santolik, N. Cornilleau-Wehrlin, M. Maksimovic, and C. C. Harvey (2003), Source location of chorus emissions observed by Cluster, *Ann. Geophys.*, *21*, 473–480.

Pontius, D. H., Jr., T. W. Hill, and M. E. Rassbach (1986), Steady state plasma transport in a corotation-dominated magnetosphere, *Geophys. Res. Lett.*, *13*(11), 1097–1100, doi:10.1029/GL013i011p01097.

Ronnmark, K. (1982), WHAMP waves in a homogeneous, anisotropic, multi-component plasma, *Rep. 179*, Kiruna Geophys. Inst., Sweden.

Ronnmark, K. (1983), Computation of the dielectric tensor of a Maxwellin plasma, *Plasma Phys.*, *25*, 699–701, doi:10.1088/0032-1028/25/6/007.

Rymer, A. M., et al. (2007), Electron sources in Saturn's magnetosphere, *J. Geophys. Res.*, *112*, A02201, doi:10.1029/2006JA012017.

Rymer, A. M., B. H. Mauk, T. W. Hill, C. Paranicas, D. G. Mitchell, A. J. Coates, and D. T. Young (2008), Electron circulation in Saturn's magnetosphere, *J. Geophys. Res.*, *113*, A01201, doi:10.1029/2007JA012589.

Santolik, O., and M. Parrot (1996), The wave distribution function in a hot magnetospheric plasma: The direct problem, *J. Geophys. Res.*, *101*(A5), 10,639–10,651, doi:10.1029/95JA03510.

Santolik, O., D. A. Gurnett, J. S. Pickett, M. Parrot, and N. Cornilleau-Wehrlin (2004a), A microscopic and nanoscopic view of storm-time chorus on 31 March 2001, *Geophys. Res. Lett.*, *31*,L02801, doi:10.1029/2003GL018757.

Santolik, O., D. A. Gurnett, and J. S. Pickett (2004b), Multipoint investigation of the source region of storm-time chorus, *Ann. Geophys.*, *22*, 2555–2563.

Thorne, R. M., T. P. Armstrong, S. Stone, D. J. Williams, R. W. McEntire, S. J. Bolton, D. A. Gurnett, and M. G. Kivelson (1997), Galileo evidence for rapid interchange transport in the Io torus, *Geophys. Res. Lett.*, *24*, 2131–2142, doi:10.1029/97GL01788.

Trakhtengerts, V. Y., A. G. Demekhov, E. E. Titova, B. V. Kozelov, O. Santolik, D. Gurnett, and M. Parrot (2004), Interpretation of Cluster data on chorus emissions using the backward wave oscillator model, *Phys. Plasmas*, *11*, 1345–1351, doi:10.1063/1.1667495.

Young, D. T., et al. (2004), Cassini plasma spectrometer investigation, *Space Sci. Rev.*, *114*, 1–112, doi:10.1007/s11214-004-1406-4.

A. J. Coates, University College London, Mullard Space Science Laboratory, Dorking, Surrey RH5 6 NT, UK.

D. A. Gurnett, G. B. Hospodarsky, J. D. Menietti, and A. M. Persoon, Department of Physics and Astronomy, University of Iowa, Van Allen Hall, Iowa City, IA 52242-1479, USA.

A. M. Rymer, Johns Hopkins University Applied Physics Laboratory, Laurel, MD 20707, USA.

O. Santolik, Charles University, KEVF MFF, V. Holesovickach 2, Praha 8, Prague, CZ-18000, Czech Republic.

D. T. Young, Southwest Research Institute, 6220 Culebra Road, San Antonio, TX 78284, USA.